JOURNAL OF AVIATION

e-ISSN: 2587-1676 J Aviat 2020; 4(1): 22-30

Research Article DOI : 10.30518/jav. 681037

Unmanned Aerial Vehicle Production with Additive Manufacturing

Ebubekir KOÇ[1], *Cemal Irfan ÇALIŞKAN*[2]*, *Mert COŞKUN*[3], *Hamaid Mahmood KHAN*[4]

Fatih Sultan Mehmet Vakif University, Aluteam, Istanbul, 34445, Turkey

Unmanned Aerial Vehicle Production with Additive Manufacturing

Abstract

In this study, unmanned aerial vehicle (UAV) design, analysis and production was made using selective laser sintering (SLS) system. Four different aircraft bodies were designed in the interdisciplinary project, one of the models was selected by comparing the computational fluid dynamics (CFD) analysis results. According to the numerical study, the model 4 design was found to be the most suitable among the tested models, then the design was produced with the SLS system. Finally, the actual flight test was carried out in three different weather conditions, and the results are presented here.

Keywords: Aviation, Additive Manufacturing, SLS, UAV, Fluent.

1. Introduction

The additive manufacturing (AM) method, also known as rapid prototyping, was first introduced in the 1980s [1]. The AM methodology is now extensively used in various sectors employing a wide range of materials. AM can be categorized into several processes depending on the adopted methodology or type of material and one such technology is selective laser sintering (SLS) [2]. The SLS process is a powder-based version of AM where low-intensity laser power is used to scan the powder particle particularly polymers, to melt their outer surface and fuse them together to form complex three-dimensional structures[3–5]. In the present study, the prototype production was performed using polyamide powder, PA2200. The production is described as follows:

In producing parts using the SLS process, a Computer-Aided Design (CAD) model is needed, which can be created using any available CAD software. The CAD file is then saved in STL (Stereolithography) or similar formats. The STL file, which is positioned according to the part sensitivity, is separated into layers by the slicing process and sent to the production system. The production process takes place within a certain systematic [6]. The parts produced using the SLS

Corresponding Author: Cemal Irfan Caliskan cemalirfancaliskan@gmail.com

Citation: Koç E., Çalışkan C.I., Çoşkun M., Khan H.M. (2020). Unmanned Aerial Vehicle Production with Additive Manufacturing J. Aviat. 4 (1), 22-30.

ORCID: [1] https://orcid.org/0000-0002-9069-715X; [2] https://orcid.org/0000-0003-0366-7698; [3] https://orcid.org/0000-0003-3307-982X [4] https://orcid.org/0000-0002-7523-4384

DOI: https://doi.org/10.30518/jav.681037

Received: 28 January 2020 **Accepted:** 30 May 2020 **Published (Online):** 22 June 2020

process are strongly dependent on the parameters are chosen so as to attain high densification and attainable mechanical and microstructural properties. In this part of the study (Table 1), some design parameters belonging to the production system EOS P110, in which UAV prototype production is taken into consideration during the design process are shared [7, 8].

Table 1. SLS design parameters considered in UAV study.

SLS Design Parameters
While printing a thin wall, the size shouldn't be smaller than 0.45 mm.
When printing supported wires, should not be thinner than 0.8mm.
The minimum size shouldn't be lower than 0.5 mm in height and 0.2 mm in width.
Escape holes need to be cleared from the un-sintered powder. The minimum diameter for the hole is 4.0 mm.
The chamber size is 193x242x322 mm.
There should be a gap of 0.1 mm between adjacent parts.
The sensitivity and the position of the SLS parts should be evaluated prior to production.

2. UAV Main Body Design Process

Biomimicry is the preferable approach to design Unmanned Aerial Vehicle (UAV). It is believed that the design created by the inspiration of flying goose will facilitate the design process in terms of aerodynamics [9]. The CAD model, including the interior and the exterior surfaces of all the UAVs, are designed in accordance with the SLS design limitations. The general form of all the UAVs is designed using the sizes given in Figure 1, which includes the wing size of 186 mm x 1470 mm, the fuselage of 110 mm x 400 mm, and a tail of 117 x 405 mm. On the tail wing located between the double vertical stabilizer, there is a controllable flap that serves during the climb and landing of the aircraft.

The right and left ailerons on the main wing serve in the airborne rotation of the aircraft.

The design consists of 32 parts, which are joined using pins. The assembly geometry allows an easy replacement of the battery, maintenance of electronic parts, or replacement of any damaged parts. The electronic components, such as motor and the control unit, are selected from the standard products. The scope of the study includes the design, analysis and the production of the demountable unmanned aerial vehicle body using the SLS machine.

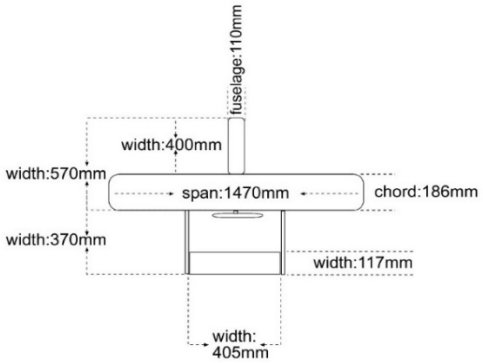

Figure 1. UAV measure sketch and wing surface area study.

The UAV includes four servo motors which one for the front wheel rudder movement, the other for the right and left-wing ailerons, and one for the tail.

The propeller motor has a total load-carrying capacity of 1.8 kg. The PA2200 powder material was used in the production of the parts using SLS process. The sintered density of the polyamide material is 0.92 g/cm3. The total weight is supposed not to exceed 1.8 kg, which is the limit set for the motor casing. The resulting UAV design has a bodyweight of 1240 gr.

The designing of the main body of the 4 different models is carried out in two stages. The modeling of the UAV model was carried out in Catia V5©: At first, the main body was created using the part design module, "multi-section solid" command. Later, the inner part of the model is emptied using the "shell" command to obtain a 0.8 mm thick shell, as shown in Figure 2.

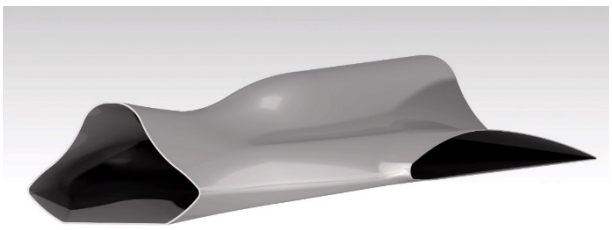

Figure 2. The outer shell modelled with the part design module in the Catia V5©.

Next, the internal modeling was carried out using CATIA V5 ©, a generative shape design module. Using the "extract" (point continuity) command, the outer surface is selected and pulled to form the internal structure, as shown in Figure 3.

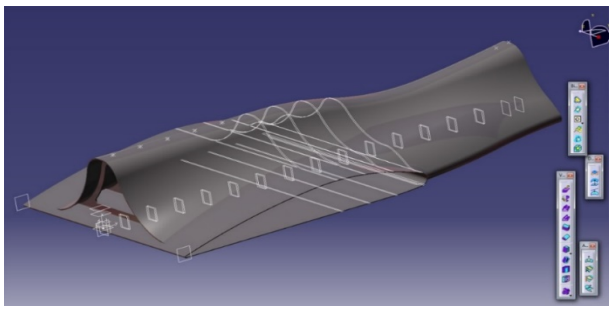

Figure 3. Internal frame modelling with generative shape design module in Catia V5©.

The cross-sections obtained in the generative shape design module are converted into solid sections in binary sections using the multi-section solid command. In Figure 4, each vertical section of the inner structure is 1 mm thick. As a result, four different models were created, as shown in Figure 5, which were then used for the CFD analysis to evaluate the pressure plots for the final production and design analysis.

Figure 4. Internal structure modelling in Catia V5©.

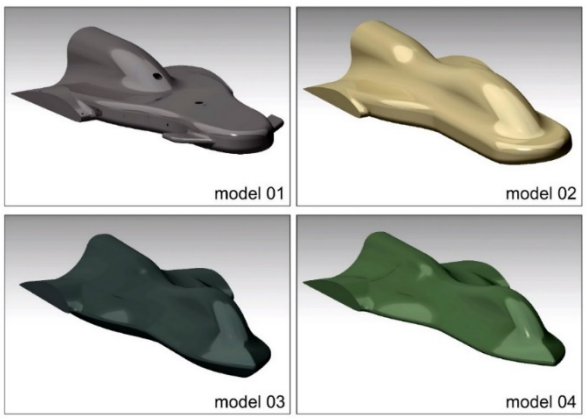

Figure 5. Four different models created during the design study.

3. UAV Main Body Design Analysis

After the preliminary design of the four CAD models of unmanned air vehicle (UAV) in CATIA, as described in the previous section, the design compatibility was realized using the ANSYS FLUENT CFD solver. At first, the CFD analysis was carried out on all the four different UAV models during taxiing using the only nose configuration (without wings). The objective was to evaluate the pressure and velocity distribution across the frame of the four models. Following this, the suitable model was selected for final CFD analysis and then physically analysed after the design and production using the SLS processes.

The first stage in the computational analysis was the preparation of a numerical model, which includes the mesh generation the formulation of solution constraints, and the mathematical model [10,12]. The UAV domain was covered by an enclosure of sufficient size such that the inlet, the outlet, and the wall of the enclosure were far from the UAV domain. This is to allow the full development of the upstream and downstream flows for effective analysis. In order to attain the low power consumption, high endurance, and improved flight performance, the CFD analysis was used to compare and evaluate the aerodynamic efficiency (C_L/C_D) and to measure the pressure and velocity distribution on the surface of the UAVs.

3.1 UAV Main Body Mesh Generation

A suitable mesh size of all the four CAD models was created using the unstructured configuration for computational analysis. Cutcell mesh was used in the study. Since the results will be obtained on the outer surfaces of the Cutcell mesh structure, it was paid attention to throw higher quality meshes on the outer borders of the models.

While constructing a mesh, a special focus was made on the mesh quality of the viscosity-affected near-wall region of the surface of the UAV. Thus, an intermediate and a fine quality three-dimensional mesh were created for the full UAV models having approximately over 4 million elements. A sufficiently large number of elements were selected in constructing the mesh for all the UAV models such that the models are indifferent to grid density and the maximum computed value of the wall unit, y+, approaches to 1 [13]. An efficient grid density from the surface of the model to the far-off region is

necessary to conserve the computational time and to enhance the accuracy of the results at the interface of the solid models. Table 2 shows the mesh parameters utilized in this study for the four models. The quality of the mesh and the total number of grid elements are also presented in the table. The values in Table 2 were determined according to the mesh parameters to which the analysis results of four different bodies were fixed. Four different body structures were analyzed under the same conditions, by determining mesh qualities and mesh parameters as close as possible.

Table 2. Mesh parameters chosen for the four UAV models, including the mesh quality and a number of elements and nodes generated.

	Model 1	Model 2	Model 3	Model 4
Global size (mm)	10.3	11.4	11.5	11.4
Element body size (mm)	4	4	4	4
Inflation layers	5	5	5	5
Growth rate	1.2	1.2	1.2	1.2
Element quality	0.998	0.966	0.962	0.962
Orthogonal quality	0.996	0.989	0.992	0.992
Skewness	0.003	0.02	0.019	0.017
Nodes (millions)	4.7	4.2	4.1	4.1
Elements (millions)	4.6	4.2	4.0	4.0

It is seen that the mesh values given in Table 2 are of high quality and skew rate.

3.2 Boundary Conditions

For each case, the free-stream velocity at the input was set at 100 m/s horizontally at zero angle of attack under standard atmospheric pressure and temperature. The zero angles of attack are chosen because the UAV models were initially analyzed during the taxiing so as to evaluate the pressure and velocity distribution. The outflow boundary conditions were set at zero pressure for the exit downstream flow.

One of the most important parameters in the selection of the turbulence model is the Reynolds number. In the formula below, how the Reynolds number is calculated is given.

$$Re=\frac{Vc\rho}{\mu} \qquad [14]$$

In the formula, V value flow rate; c is the chord width value; ρ represents the density of the flow used and μ represents the kinematic viscosity value. When the boundary condition and the data determined as standard were calculated in the formula V = 100 m / s, c = 0, 18644 m, ρ = 1,225 kg / m3, μ = 17894x10-5 kg / m.s Reynolds number (Re) = 1.276.334.

The turbulence modeling in transitional flows was obtained using the $k-\omega$ SST transitional model. This turbulence model is the most suitable one used in many studies, as observed here [15, 16].

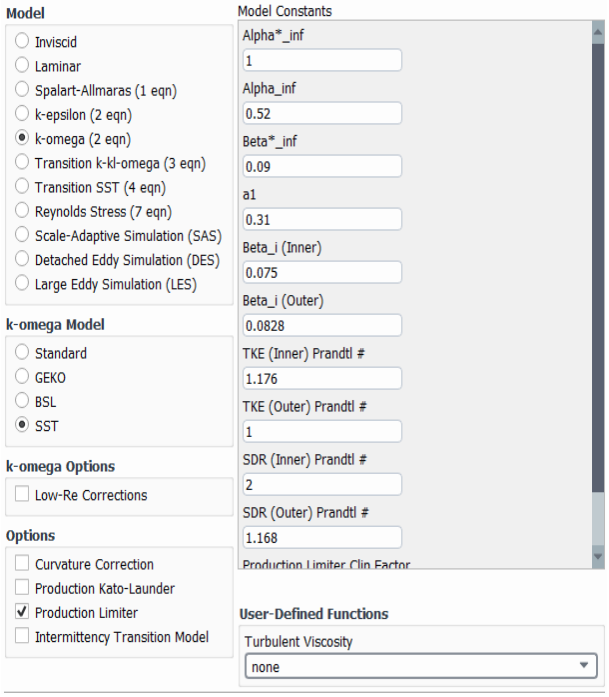

Figure 6. Defining the k − ω turbulence model

3.3 Results and comparison of the CFD analysis of the 4 UAV models

Table 3 shows the results of the aerodynamic variables of all the 4 UAV models. The maximum pressure and velocity parameters of all the tested models were found nearly similar. Out of the 4 different models, the pressure distribution can be seen maximum on the nose of the model 1 that

represents a high resistance during taxiing. Therefore, the model 1 was not undertaken for further analysis. Moreover, the low drag and high lift coefficient in aircraft are preferred for higher efficiency and endurance strength, which was found comparatively better in model 4. Also, the high C_L/C_D ratio in model 4 suggests the higher aerodynamic efficiency, which is a critical parameter in the designing of the aircraft models. Based on the initial CFD analysis of all the UAVs during taxiing, model 4 was chosen for further analysis, including production and a physical flight test.

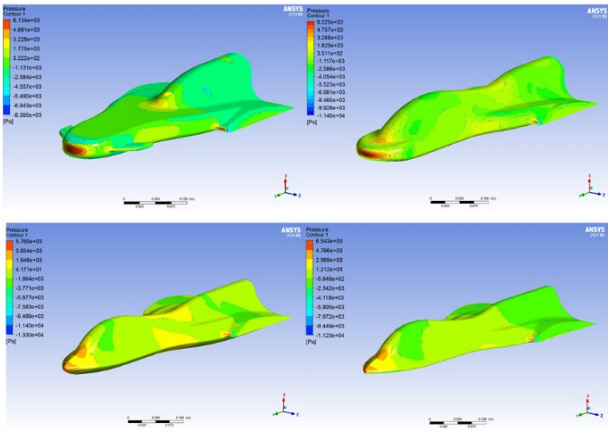

Figure 7. Velocity and pressure distribution on the four models.

Table 3. The maximum pressure and velocity values obtained from the four models.

	Model 1	Model 2	Model 3	Model 4
Max pressure (KPa)	6.5	6.6	6.5	6.6
Max velocity (m/s)	135.7	143.7	138.9	141.5
Drag coefficient (C_D)	0.03	0.024	0.019	0.020
Lift coefficient (C_L)	0.046	0.05	0.009	0.048
C_L/C_D	1.53	2.06	0.48	2.44

As seen from the Table 2, model 4 exhibits the low drag and high lift coefficient. This suggests the higher efficiency and endurance strength in model 4 compared to all the other models. Moreover, the high C_L / C_D ratio in model 4 suggests the higher aerodynamic efficiency, which is important in designing the aircraft models. Based on the initial CFD analysis of all the UAVs during taxiing, the model 4 was observed to be the best prototype for the final design, production, and flight test.

The relevant formulas for calculating the drag coefficient (C_D) and lift coefficient (C_L) values were given below. CFD softwares provide analysis results related to the background running of these formulas.

$$C_D = \left(\frac{F_D}{\frac{1}{2}A\rho V^2}\right) \quad [17]$$

$$C_L = \left(\frac{F_L}{\frac{1}{2}A\rho V^2}\right) \quad [17]$$

The maximum pressure and maximum speed values in Table 3 were automatically calculated in the analysis program by entering the boundary conditions and standard. These values obtained automatically on the program should be changed in the reference values section.

4. UAV Model 04 Body Parts Design

In the aviation, the analysis of the model is as important as the design processes. Aerodynamic simulation studies on the pre-production verification of the designed model can take a long time [18]. The results of the analysis play an effective role in determining the deficiencies of the process before the production stage.

According to the results of the pressure distribution on the main body, model 4 was found to be in the ideal design (Figure 7). During the detailed design process, it was decided to continue with model 4 due to ease of design and production. In addition, model 4 offers more space to create the space required for battery and electronic components.

In our UAV study, the “measure inertia” command in the submenu of the Catia V5 © was used to determine the balance point of the aircraft. Accordingly, the weight of the electronic parts and the battery was measured, which are located in the nose section. For easy charging and maintenance related issues, the base of the nose section was connected to the main body using the carbon fiber

rods. The upper section was modeled as a sliding cover and then fixed with m3 screw. While the black part in Figure 8 represents the battery compartment in the form of a sliding cover, the bottom grey part is the main part of the aircraft section, where the landing gear is attached.

Figure 8. Model 4 nose form, battery compartment design. The black and grey sections represent the sliding cover and the fixed section, respectively.

5. UAV Wing Design

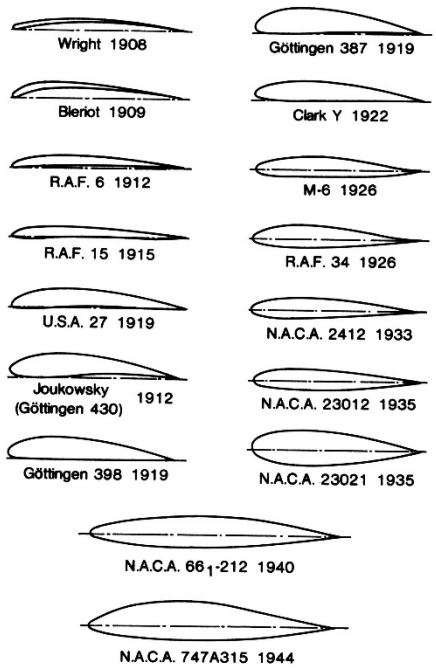

Figure 9. Airfoil used to determine wing form "göttingen 398 1919" and other airfoil forms [19].

After the main body design, the wing design for model 4 was carried out. According to the literature, the wing form, Göttingen 398 1919 (Figure 9), for the model was chosen because of its suitability to the existing design. The connection between the different parts of the wings was achieved using the modeled spacers and pins. For the attachment of the wing with the mainframe, a carbon fiber rod of 7 mm diameter was used at the front of the wings. Intra-wing carbon fiber rod reinforcement method is widely used in the literature [20]. The wing for the UAV model was made up of four different parts. In addition, gaps for servo motors were also designed on the outer wings.

In general, the outer shell in the wing design was modeled with a thickness of 0.55 mm. Vertical carriers in the form of the airfoil in the inner frame were 1 mm thick. The wings, which were designed in flat features, consist of extruding airfoil form (Figure 10) with a shell size of 0.55 mm. The perforated wing repeats along the wing at 20 mm intervals. Finally, the movable parts in the outer wings were modeled together with a tolerance of 0.5 mm using the hinge cylinders, and the parts (wing and aileron) were used directly without any post-production assembly.

Figure 10. Inner wing design.

6. UAV Model 04 Detail Designs

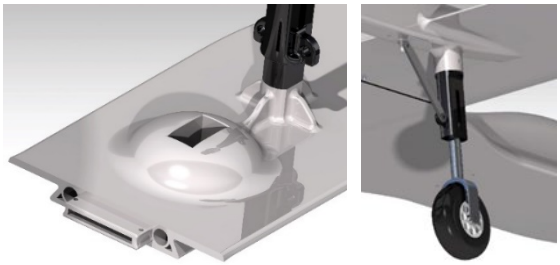

Figure 11. Landing gear mount detail, and nose servo gap.

After modeling the wing design as 4 main parts and 2 aileron, servo gaps and landing gear were designed, as shown in Figure 11. Internal ducts or suitable gaps were created for the wirings of servo motors. Moreover, the part design module of CATIA was used in the designing of landing gear and wheels. It was tested that if the tires to be used on wheels are produced with polyamide, they do not provide the required damping; Thus, the tires were

supplied from products produced for the ready model (Figure10). For the front and the rear landing gear, the wheel diameter was chosen 50 mm. A 2.8 mm diameter pins or m3 screws were used for the assembly of landing gear and the other parts. Also, in the design of the landing gear, a spring of suitable flexibility was used to provide necessary damping during the landing of the UAV.

7. UAV Model 04 Simulation

In order to have a detailed understanding of model 4 during the flight, the wings were added to the UAV in CATIA, and the final model was simulated under similar conditions, as described in the previous section. The quality of the mesh is extremely important for accurate results. Therefore, the UAV frame was cut into half and simulated using a symmetric plane to conserve computational time and to increase accuracy. An unstructured cut-cell mesh with about 4.1 million elements was applied on the half body of the model 4, as shown in 12.

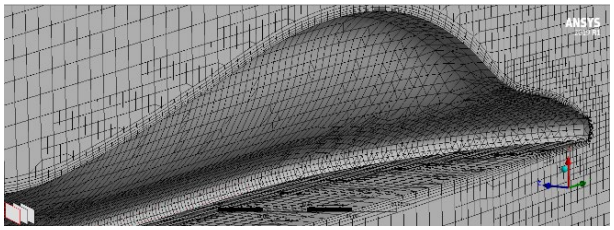

Figure 12. Mesh quality in and around the frame of the nose region.

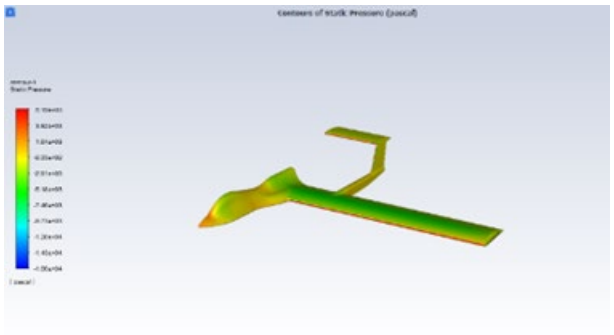

Figure 13. The pressure distribution of the half model.

The grid independence study was carried out initially such that the results of the analysis remain the same regardless of any further variance in the mesh structure. At first, an unstructured standard mesh with about 1.5 million elements was used to calculate the lift and drag coefficients. Later, the mesh was refined by introducing body sizing at the mainframe, and the lift and drag values were calculated subsequently. The change in C_L and C_D was noticed until the total elements reached 4 million for the half body. The selected mesh is shown in Figure 12 and presented in Table 4.

Table 4. Mesh quality and results of model 4 with wings.

	UAV model 4 with symmetry
Mesh type	Cutcell
Inflation (layers)	5
Growth rate	1.2
Body sizing (mm)	10
Element quality	0.96
Orthogonal quality	0.99
Skewness	0.02
Nodes (million)	4.24
Elements (million)	4.12
Wing area (m^2)	0.12
Turbulence model	$k-\omega$ SST
Maximum pressure (kPa)	6.4
Maximum velocity (m/s)	137
C_D	0.04
C_L	0.5
C_L/C_D	12.21

Since the previous models were investigated without wings, the lift coefficient was observed quite low. Therefore, on adding the wings to the UAV model 4, the lift coefficient was found 0.50, a rise from 0.048 that saw a rise of nearly 900 % in values of lift coefficient. This leads to the higher C_L/C_D ratio of 12.21 against 2.44 without wings, as shown in Table 4. This signifies that the addition of wings results in higher aerodynamic efficiency. The Figure 14, 15 shows the pressure and velocity distribution on the full model and on the wings as well. The high velocity at the top of the frame compared to the bottom of the frame signify the higher lift in the CFD study.

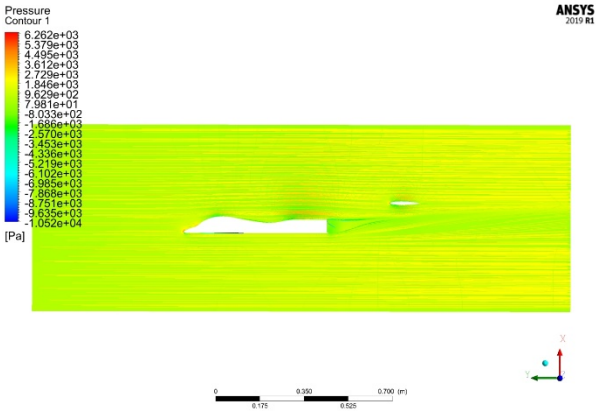

Figure 14. The pressure distribution at the full body.

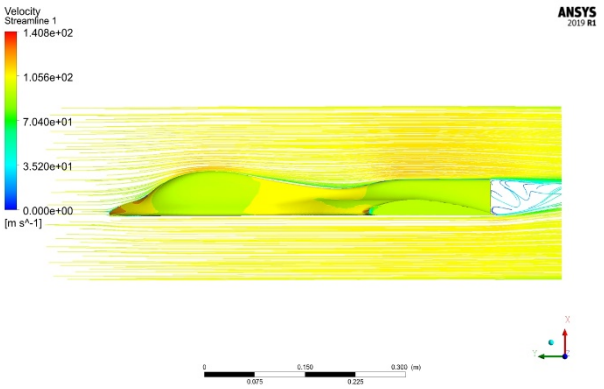

Figure 15. The velocity distribution at the full body.

8. Conclusion

Four different UAV designs were modeled using *Catia V5*© and the model was examined using CFD analysis in taxi position. The pressure plots were analysed and evaluated in terms of model efficiency and endurance using a commercial FLUENT package. Based on the analysis, model 4 was found most suitable among the different UAVs and was then chosen for further analysis. The wings were then added to the model, and the whole model was further evaluated for aerodynamic calculations for real flight conditions. Later, the different parts of the UAV were fabricated using the SLS process and assembled, as shown in Figure 16. The assembled body of the model 4 was then tested on the ground for spring flexibility with the attached landing gear. After the taxiing trails, the model was then tested in air successfully and the exercise was repeated in different weather conditions, as shown in Figure 17.

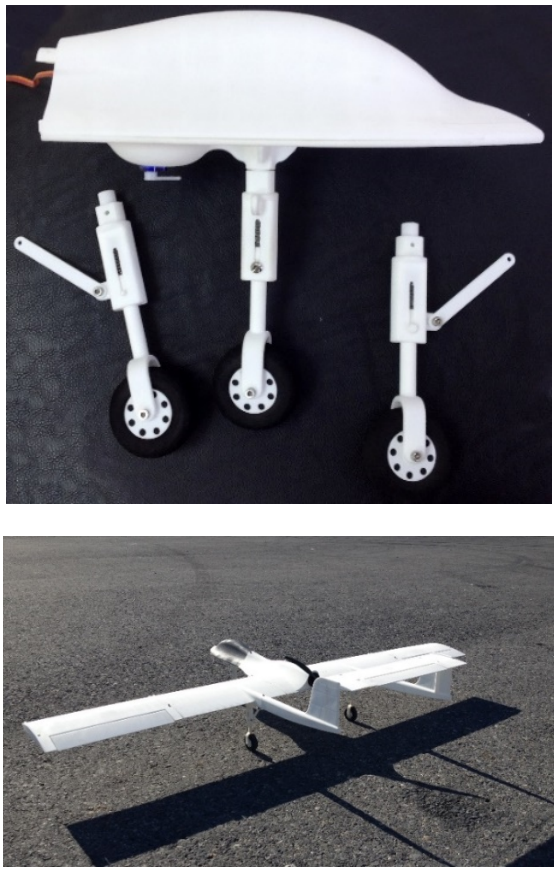

Figure 16. Parts manufactured with SLS (top) and flight tests (below).

Figure 17. Flight tests.

Acknowledgements

This study was prepared within the scope of "ALUTEAM-Aluminum Test Training and Research Center" Project supported by ISTKA (Istanbul Development Agency) Guided Project Support and "Aluminum Building Systems Testing and Training Laboratory" Project supported by ISTKA 2018-Innovative and Creative Istanbul Financial Support Program, which have been carried out by Fatih Sultan Mehmet Vakif University. We would like to thank Dr. Ali İhsan

Koca for his support in simulation and to Mark Pellowe for the calculations, and Tunahan Tez for the flight tests.

Data Availability

No data, models, or code were generated or used during the study.

Ethical Approval

Not applicable.

References

[1] K. V Wong and A. Hernandez, "A review of additive manufacturing," ISRN Mech. Eng., 4–5, 2012.

[2] S. Kumar, "Selective laser sintering: a qualitative and objective approach," Jom, 55, 10,43–47, 2003.

[3] I. Gibson, D. W. Rosen, and B. Stucker, "Design for additive manufacturing," in Additive manufacturing technologies, Springer, 2010, 299–332.

[4] J. Gardan, "Additive manufacturing technologies: state of the art and trends," Int. J. Prod. Res., 54, 10, 3118–3132, 2016.

[5] A. Nazarov, I. Skornyakov, and I. Shishkovsky, "The setup design for selective laser sintering of high-temperature polymer materials with the alignment control system of layer deposition," Machines, 6, 1, 11, 2018.

[6] C. I. Caliskan, Double Stud Air Cargo Fitting: Historical Review and Alternative Design and Prototype Manufacturing Process with Additive Manufacturing. Germany, Lambert Academic Publishing, 2019.

[7] Eos, "Printing with EOS SLS printer." 3–4, 2015.

[8] C. C. Seepersad, T. Govett, K. Kim, M. Lundin, and D. Pinero, "A designer's guide for dimensioning and tolerancing SLS parts," in Solid Freeform Fabrication Symposium, Austin, *TX*, 2012, 921–931.

[9] D. M. Bushnell, "Industrial Design in Aerospace/Role of Aesthetics," Nasa Technical Report, 20060025011, 2006.

[10] P. P. Hector Guillermo, A. M. Victor Daniel, and G. G. Elvis Eduardo, "CFD Analysis of two and four blades for multirotor Unmanned Aerial Vehicle," 2018 IEEE 2nd Colomb. Conf. Robot. Autom. CCRA 2018, January 2019, 1–6, 2018.

[11] L. Velazquez-Araque and J. Nožička, "Computational analysis of the 2415-3S airfoil aerodynamic performance," IMETI 2013 - 6th Int. Multi-Conference Eng. Technol. Innov. Proc., 12, 1, 86–91, 2013.

[12] Q. Wang, S. Wu, W. Hong, W. Zhuang, and Y. Wei, "Submersible Unmanned Aerial Vehicle: Configuration Design and Analysis Based on Computational Fluid Dynamics," MATEC Web Conf., 95, 0–5, 2017.

[13] H. A. Kutty and P. Rajendran, "3D CFD simulation and experimental validation of small APC slow flyer propeller blade," Aerospace, 4, 1, 2017.

[14] H. A. Alabaş, M. Albatran, T. Çelik, M. Lüleci, and Ü. D. Göker, "Oyuk Boşluk Yapısının Kanat Profili Üzerine Etkisi," J. Aviat., 3, 2, 89–105.

[15] S. Ren, S. Li, Y. Wang, D. Deng, and N. Ma, "Finite element analysis of residual stress in 2.25Cr-1Mo steel pipe during welding and heat treatment process," J. Manuf. Process.,47, September, 110–118, 2019.

[16] W. Wisnoe, R. Nasir, W. Kuntjoro, and A. Mamat, "Wind Tunnel Experiments and CFD Analysis of Blended Wing Body (BWB) Unmanned Aerial Vehicle (UAV) at Mach 0.1 and Mach 0.3," Int. Conf. Aerosp. Sci. Aviat. Technol., 13, 1–15, 2009.

[17] L. E. Velazquez-Araque, "Design of an of an aerodynamic measurement system for unmanned aerial vehicle airfoils," Systemics, Cybernetics and Informatics, 10, 5, 39-44, 2012.

[18] J. K. Lytle, "The numerical propulsion system simulation: A multidisciplinary design system for aerospace vehicles," Nasa Technical Report, 19990062672, 1999.

[19] N. C. Administrator, "the Naca", , https://www.nasa.gov/topics/aeronautics/features/naca2010_gallery4.html, [Erişim Tarihi: 20.06.2020].

[20] G. Nicholson and C. Roberts, "Rapid manufactured fixed wing powered uav," Univ. Sheff. Adv. Manuf. Centre, Roatherham, Technical Report, United Kingdom, 2014.